

# “Cloud slicing”: A new technique to derive upper tropospheric ozone from satellite measurements

J. R. Ziemke<sup>1</sup>

Stinger Ghaffarian Technologies, Greenbelt, Maryland

S. Chandra and P. K. Bhartia

NASA Goddard Space Flight Center, Greenbelt, Maryland

**Abstract.** A new technique called cloud slicing has been developed for measuring upper tropospheric O<sub>3</sub>. Cloud slicing takes advantage of the opaque property of water vapor clouds to ultraviolet wavelength radiation. Measurements of above-cloud column O<sub>3</sub> from the Nimbus 7 Total Ozone Mapping Spectrometer (TOMS) instrument are combined together with Nimbus 7 temperature-humidity and infrared radiometer (THIR) cloud-top pressure data to derive O<sub>3</sub> column amounts in the upper troposphere. In this study, tropical TOMS and THIR data for the period 1979–1984 are analyzed. By combining total tropospheric column ozone (referred to as TCO) measurements from the convective cloud differential (CCD) method with 100- to 400-hPa upper tropospheric column O<sub>3</sub> amounts from cloud slicing, it is possible to estimate 400- to 1000-hPa lower tropospheric column O<sub>3</sub> and evaluate its spatial and temporal variability. Results for both the upper and lower tropical troposphere show a year-round zonal wave number 1 pattern in column O<sub>3</sub> with the largest amounts in the Atlantic region (up to ~15 DU in the 100- to 400-hPa pressure band and ~25–30 DU in the 400- to 1000-hPa pressure band). Upper tropospheric O<sub>3</sub> derived from cloud slicing shows maximum column amounts in the Atlantic region in the June–August and September–November seasons which are similar to the seasonal variability of CCD-derived TCO in the region. For the lower troposphere, the largest column amounts occur in the September–November season over Brazil in South America and also southern Africa. Localized increases in the tropics in the lower tropospheric O<sub>3</sub> are found over the northern region of South America around August and off the west coast of equatorial Africa in the March–May season. Time series analysis for several regions in South America and Africa show an anomalous increase in O<sub>3</sub> in the lower troposphere around the month of March which is not observed in the upper troposphere. The eastern Pacific indicates weak seasonal variability of upper, lower, and total tropospheric O<sub>3</sub> compared with the western Pacific, which shows the largest TCO amounts in both hemispheres around spring months. O<sub>3</sub> variability in the western Pacific is expected to have greater variability caused by strong convection, pollution and biomass burning, land-sea contrast, and monsoon developments.

## 1. Introduction

The determination of ozone (O<sub>3</sub>) in the troposphere from satellite retrievals has a growing history beginning with *Fishman et al.* [1990]. In that study a residual method was used where the total column of tropospheric ozone (hereinafter referred to as tropospheric column ozone, or TCO) was derived by subtracting stratospheric column ozone (SCO) (via the Stratospheric Aerosol and Gas Experiment (SAGE)) from total column ozone (via the Total Ozone Mapping Spectrometer (TOMS)). Because of the sparse temporal and spatial coverage of SAGE data, the derived fields of SCO and TCO were best suited for studying seasonal cycle climatologies. *Fishman et al.* [1996] and *Vukovich et al.* [1996] estimated daily fields of TCO. Both of these investigations used solar back-

scattered ultraviolet (SBUV) O<sub>3</sub> measurements to derive SCO. In the study by *Vukovich et al.* [1996], extensive comparisons were made with ground-based measurements, and significant discrepancies were noted. Because of the nature of the SBUV retrieval algorithm, O<sub>3</sub> disturbances in the troposphere propagate into the SCO fields, producing noise and data artifacts in determined residual fields of TCO. A new and improved approach to using SBUV data for deriving SCO and TCO was shown by *Fishman and Balok* [1999] in which SBUV data were adjusted using ozonesonde data. The method proved useful for determining daily regional maps of TCO outside the tropics for tracking pollution events.

*Hudson and Thompson* [1998] proposed a modified residual method for the tropics which combined TOMS and ozonesonde measurements. Their method assumes that the longitudinal variation of total column O<sub>3</sub> at the equator consists of an underlying wave number 1 structure with superimposed smaller-scale fluctuations which they characterize as “excess ozone” and attribute primarily to biomass burning. The wave number 1 structure is assumed to consist of a zonally invariant strato-

<sup>1</sup>Also at NASA Goddard Space Flight Center, Greenbelt, Maryland.

spheric component and a tropospheric component consisting of a constant background and a zonally varying wave number 1 component. The latter is determined by fitting a sinusoid to total column  $O_3$  using only Pacific data, which are then subtracted from the total column  $O_3$  to estimate "excess ozone." Unfortunately, the nonfluctuating component of tropospheric  $O_3$  cannot be uniquely determined from TOMS measurements alone and must be evaluated using another set of  $O_3$  measurements. However, it needs to be evaluated at only one longitude to calculate SCO, which is assumed to be zonally invariant. Hudson and Thompson [1998] used ozonesonde data from a number of stations in the Atlantic region and concluded that for the 1991–1992 time period, the nonfluctuating component of tropospheric  $O_3$  in this region had a mean value of about 24 DU with an additional seasonal variability of around 5-DU amplitude. They further assumed that these values do not change from year to year. The modified residual method may thus not fully account for the interannual variability of tropospheric  $O_3$ , which is driven largely by El Niño and La Niña events in the Pacific [Chandra *et al.*, 1998]. The data may be best suited for the Atlantic region [Thompson and Hudson, 1999].

Ziemke *et al.* [1998] introduced two new methods for deriving TCO in the tropics. The first was to use assimilated Microwave Limb Sounder (MLS) and Halogen Occultation Experiment (HALOE) SCO measurements to derive TCO. This was a residual method similar to that of Fishman *et al.* [1990] and used TOMS measurements of total column  $O_3$ . The advantage of this approach is that daily maps of high spatial coverage can be obtained. The main limitation of this approach was the combination of two stratospheric instrument measurements with TOMS total  $O_3$ , resulting in sizable interinstrument calibration errors in calculated TCO. The second approach for deriving TCO by Ziemke *et al.* [1998] used optically thick convective clouds, hereinafter referred to as the convective cloud differential (CCD) method. This second method was limited to the tropics because it required persistent high-reflectivity tropopause-level clouds to develop month-to-month gridded time series. In the CCD method, total column  $O_3$  is derived from low-reflectivity ( $R < 0.2$ ) measurements, and SCO follows from nearby column  $O_3$  measurements taken above the tops of very high tropopause-level clouds under conditions of high reflectivity ( $R > 0.9$ ). First, above-cloud column amounts are calculated in the Pacific region where tropopause-level clouds are persistent. SCO is then derived for every  $5^\circ$  latitude band and averaged from  $120^\circ\text{E}$  eastward to  $120^\circ\text{W}$  using only the lowest values of above-cloud column amounts (the lowest values coincide with tropopause-level cloud tops). These SCO values are then assumed to be independent of longitude in a given latitude band. This assumption is based on the characteristics of zonal symmetry of tropical SCO as inferred from Upper Atmosphere Research Satellite (UARS) MLS and HALOE ozone data. We refer the reader to Ziemke *et al.* [1998] for further details regarding the CCD technique. A unique property of the CCD method for deriving TCO is that it is not affected by interinstrument calibration errors because it uses only TOMS measurements. For the CCD TCO data used in this study, several corrections were made including adjustments for sea glint, tropospheric aerosols, and retrieval efficiency problems in the lower troposphere. These data corrections are discussed in detail in Appendix A.

All of the previous methods using satellite data could only provide estimates of the total column of  $O_3$  in the troposphere.

### Using Cloud Tops To Obtain Mean $O_3$ Volume Mixing Ratio

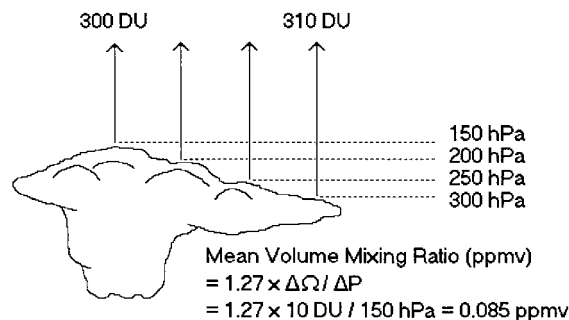


**Figure 1.** Illustration of cloud slicing for the case of high-resolution measurements of above-cloud column  $O_3$  and cloud-top pressures. The figure shows numbers indicating an  $O_3$  mixing ratio of 85 ppbv in the upper troposphere, which is an amount often found in midlatitudes or in polluted tropical environments. The numbers shown in this figure are for illustration only.

The present study uses a new technique called cloud slicing to derive tropospheric  $O_3$  profile information in the tropics from satellite measurements. Cloud slicing in this investigation will be shown to be capable of providing time series of upper and lower tropospheric column  $O_3$  from satellite retrievals when combined with TCO measurements.

## 2. Overview of Cloud Slicing

The cloud-slicing method for measuring  $O_3$  is an extension of the CCD technique of Ziemke *et al.* [1998] for measuring TCO. The technique used in cloud slicing is shown in Figure 1. With this method, colocated measurements of above-cloud column  $O_3$  and cloud-top pressure are combined to yield tropospheric  $O_3$  profile information. Given a database of these two colocated measurements, the derivation of the  $O_3$  profile information is then straightforward. Column  $O_3$  ( $\Omega$ ) between two pressure surfaces  $P_{\text{low}}$  and  $P_{\text{high}}$  ( $P_{\text{low}} < P_{\text{high}}$ ) in the troposphere can be derived by integrating  $O_3$  volume mixing ratio ( $X$ ) over pressure from  $P_{\text{low}}$  to  $P_{\text{high}}$ :

$$\Omega = A \int_{P_{\text{low}}}^{P_{\text{high}}} dP X, \quad (1)$$

where  $\Omega$ ,  $P$ , and  $X$  are in Dobson units (DU), hectopascals, and ppmv, respectively, and  $A$  is a constant equal to  $\sim 0.79 \text{ DU hPa}^{-1} \text{ ppmv}^{-1}$  for the troposphere (see Appendix B).

From (1) a mean volume mixing ratio (VMR, in ppmv) for  $O_3$  in this same pressure interval is given by

$$\bar{X} = 1.27 \times \frac{\Delta\Omega}{\Delta P}. \quad (2)$$

The distribution of  $O_3$  derived from (2) reflects all natural changes in  $O_3$  in the real atmosphere. The  $O_3$  amounts obtained from (2) make no assumptions regarding the state of the atmosphere of being well mixed or having no net sources or sinks for  $O_3$ .

Figure 1 illustrates high-resolution cloud slicing where satellite field-of-view (FOV) footprint measurements are small

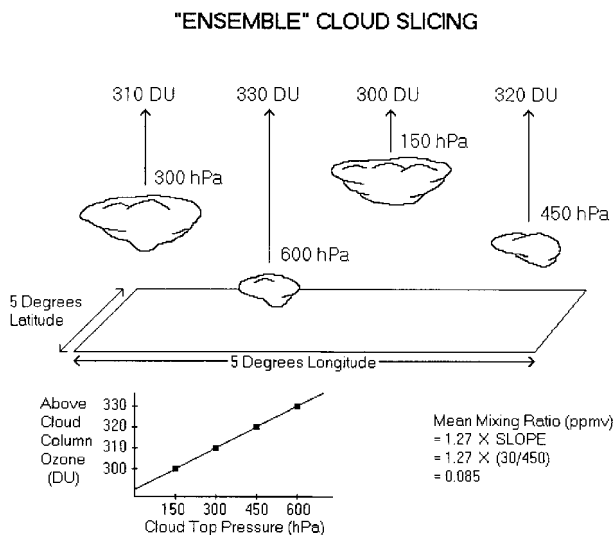


**Figure 2.** Illustration of the statistical ensemble approach used in the study with cloud slicing for deriving tropospheric  $O_3$  abundances. The lower part of the figure indicates that when above-cloud column  $O_3$  is plotted versus cloud-top pressure for a well-mixed atmosphere with constant  $O_3$  volume mixing ratio (VMR), one ideally obtains a straight line. The values given for above-cloud column  $O_3$  amounts and cloud-top pressures are for illustration only.

enough to provide cloud-slicing analysis of individual clouds. TOMS measurements, however, have a large FOV footprint (about 100 km, on average) which is often larger than the clouds being used for cloud slicing. The result is often not enough clouds and too much clear sky in the FOV measurements.

This pilot study of cloud slicing uses a statistical ensemble approach (see Figure 2) for measuring tropospheric  $O_3$  by combining many collocated measurements of cloud-top pressure and above-cloud column  $O_3$  over a broad region ( $5^\circ \times 5^\circ$  bins). This analysis was carried out for monthly ensembles, and to reduce the number of partially cloudy footprint scenes, only TOMS  $O_3$  measurements with reflectivity  $R$  greater than 0.6 were used in the cloud-slicing analyses. Scenes with  $R > 0.6$  coincide with 100% cloud fraction [Eck *et al.*, 1987] and generally middle to upper tropospheric cloud tops [Stowe *et al.*, 1989]. Once mean VMR is derived, column  $O_3$  follows by inverting (2) to solve for  $\Delta\Omega$  (for example,  $\Delta\Omega = 0.79 \times \bar{X} \times 300$  hPa for 100- to 400-hPa mean column  $O_3$ ). The  $R > 0.6$  filtering not only reduces the amount of clear-sky contamination but also reduces or eliminates problems such as efficiency factor, sea glint, and tropospheric aerosols that can all seriously affect cloud-slicing measurements (see Appendix A). Because of a relatively small number of  $R > 0.6$  cloud tops and reduced ozone retrieval efficiency in the lower troposphere, our study derives gridded time series of mean upper tropospheric VMR (and corresponding  $O_3$  column) in the 100-hPa ( $\sim 17$  km altitude) to 400-hPa ( $\sim 8$  km altitude) pressure band. All data in this study were binned to equivalent  $5^\circ$  latitude by  $5^\circ$  longitude block structures centered at latitudes  $12.5^\circ\text{S}$ ,  $7.5^\circ\text{S}$ , ...,  $12.5^\circ\text{N}$ , and longitudes  $177.5^\circ\text{W}$ ,  $172.5^\circ\text{W}$ , ...,  $177.5^\circ\text{E}$ .

This study combines collocated measurements of Nimbus 7 temperature-humidity infrared radiometer (THIR) cloud-top pressure and Nimbus 7 TOMS column  $O_3$  for the time period

1979–1984. The Nimbus 7 TOMS  $O_3$  data are version 7, level 2, footprint measurements [e.g., McPeters *et al.*, 1996]. The Nimbus 7 THIR instrument [Stowe *et al.*, 1988] is a two-channel scanning radiometer measuring Earth radiation from two spectral bands,  $10.5\text{--}12.5\ \mu\text{m}$  ( $11.5\ \mu\text{m}$  mean) and  $6.5\text{--}7.0\ \mu\text{m}$  ( $6.7\ \mu\text{m}$  mean). The  $6.7\text{-}\mu\text{m}$  band provides measurements of moisture in the middle and upper troposphere, and the  $11.5\text{-}\mu\text{m}$  band provides cloud-top temperatures. Cloud-top pressures were derived from THIR cloud-top temperatures using data from National Centers for Environmental Prediction (NCEP).

Our study utilizes only optically thick 100% cloud-filled scenes. Stowe *et al.* [1988] indicated RMS  $1\sigma$  uncertainties in THIR measured cloud-top temperatures of about 1–1.5 K in the upper troposphere for optically thick clouds. From upper tropospheric tropical sonde measurements (not shown), 1 K corresponds to an approximately 5- to 10-hPa pressure change. THIR temperature measurement uncertainties of 1–1.5 K then correspond to cloud-top pressure errors of around 10–15 hPa. Additional error in cloud-top pressure arises from the conversion of cloud-top temperature to cloud-top pressure from the NCEP analyses. Basist *et al.* [1995] and Basist and Chelliah [1997] provided comparisons of NCEP temperature data with brightness temperature measurements from the Microwave Sounding Unit (MSU) instrument. The results indicated uncertainties in NCEP temperature analyses of a few degrees Centigrade in the troposphere. If we assume RMS  $1\sigma$  uncertainties in upper tropospheric NCEP temperatures of about 2 K in the tropics, the subsequent  $1\sigma$  error in cloud-top pressure is around 20 hPa. The THIR temperature measurement error combined with the NCEP conversion error yields a  $1\sigma$  uncertainty in derived cloud-top pressure of around 25 hPa (i.e.,  $(15^2 + 20^2)^{1/2} = 25$  hPa). From tropical ozonesonde measurements (not shown) an uncertainty of 25 hPa in cloud-top pressure corresponds to an approximately 2-DU column  $O_3$  amount in the upper troposphere.

Figure 3 shows the average number of collocated footprint measurements per month of TOMS above-cloud column  $O_3$  and THIR cloud-top pressure in the 100- to 400-hPa interval over the 1979–1984 time period. The highest numbers (greater than 150) of collocated measurements lie in the western Pacific and eastern Indian Ocean, with similar high numbers ( $\sim 100$ ) over western South America, western Africa, and the North Atlantic. In this study the minimum number of collocated data pairs for any given month within any  $5^\circ \times 5^\circ$  bin was taken to be 30 in order to provide adequate statistics for developing monthly time series and seasonal cycle climatologies. Regions such as the South Atlantic and South Pacific west of South America have, on average, less than 20 data pairs per month.

### 3. Statistical Ensemble Scatter Diagrams

Figure 4 shows monthly scatterplots of TOMS  $R > 0.6$  above-cloud column  $O_3$  versus THIR cloud-top pressure for February 1981 at  $2.5^\circ\text{N}$  in the Atlantic region (top panels) and western Pacific region (bottom panels). Line fits were applied in each case to all data pairs shown with derived mean  $O_3$  VMR indicated. Each case in Figure 4 indicates a general linear relationship with significantly larger amounts of mean  $O_3$  VMR in the Atlantic than in the Pacific. Because the ensemble data in Figure 4 are accumulated over an entire month, some of the scatter in the data comes not from errors in cloud-top pressure and above-cloud column  $O_3$  but from

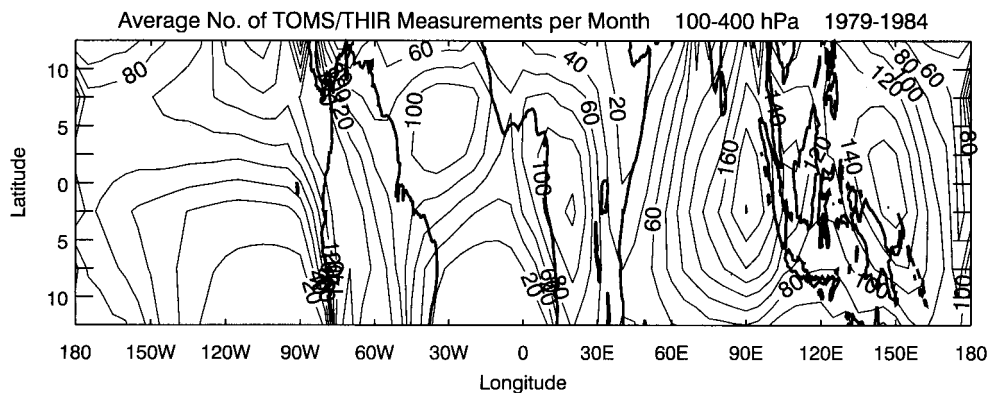


**Figure 3.** Average number of colocated footprint measurements per month of Total Ozone Mapping Spectrometer (TOMS) above-cloud column O<sub>3</sub> and temperature-humidity infrared radiometer (THIR) cloud-top pressure in the 100- to 400-hPa interval over the 1979–1984 time period.

either photochemical changes or perturbations of column O<sub>3</sub> caused by dynamical events in the stratosphere [e.g., Ziemke and Stanford, 1994]. The amplitudes in above-cloud column O<sub>3</sub> caused by these tropical disturbances (e.g., Kelvin waves, mixed Rossby-gravity wave, equatorial Rossby modes, etc.) are generally only a few Dobson units in column O<sub>3</sub>.

**4. Horizontal Distributions of Tropospheric O<sub>3</sub>**

Figure 5 shows zonal variations of CCD TCO (top curves), 400- to 1000-hPa column O<sub>3</sub> (middle curves), and 100- to 400-hPa column O<sub>3</sub> (bottom curves) at latitude 2.5°N (Figure 5a) and 2.5°S (Figure 5b). These line plots are based on a 6-year (1979–1984) climatology and are meant to illustrate

zonal and seasonal characteristics. The 400- to 1000-hPa column O<sub>3</sub> amounts were derived by subtracting 100- to 400-hPa column O<sub>3</sub> from TCO. Within statistical uncertainties, all three column measurements show a zonal wave number 1 pattern year-round with largest O<sub>3</sub> amounts in the Atlantic region. Most of the wave number 1 pattern originates in the lower troposphere, as was indicated previously by Ziemke and Chandra [1998] from tropical ozonesonde measurements. The wave number 1 distribution in Figure 5 at 2.5°N and 2.5°S is also present at other tropical latitudes, as shown by the contour plots of Plates 1–3 for 100- to 400-hPa column O<sub>3</sub>, TCO, and 400- to 1000-hPa column O<sub>3</sub>, respectively.

There are several regions in Plate 1 such as the South At-

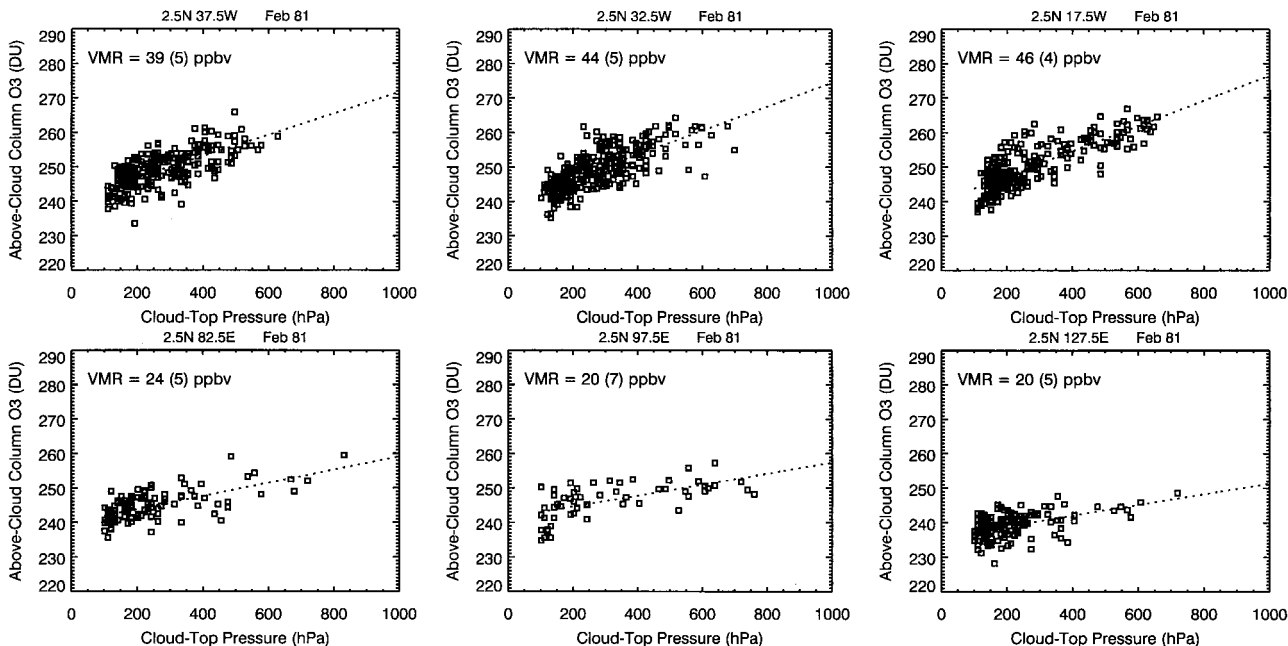


**Figure 4.** TOMS above-cloud column O<sub>3</sub> (in Dobson units) versus THIR cloud-top pressure (in hectopascals) scatterplots for the month of February 1981 over (top) the Atlantic and (bottom) the western Pacific. Indicated in each panel are line fits for estimating average VMR from cloud slicing. Statistical 2σ values are shown in parentheses.

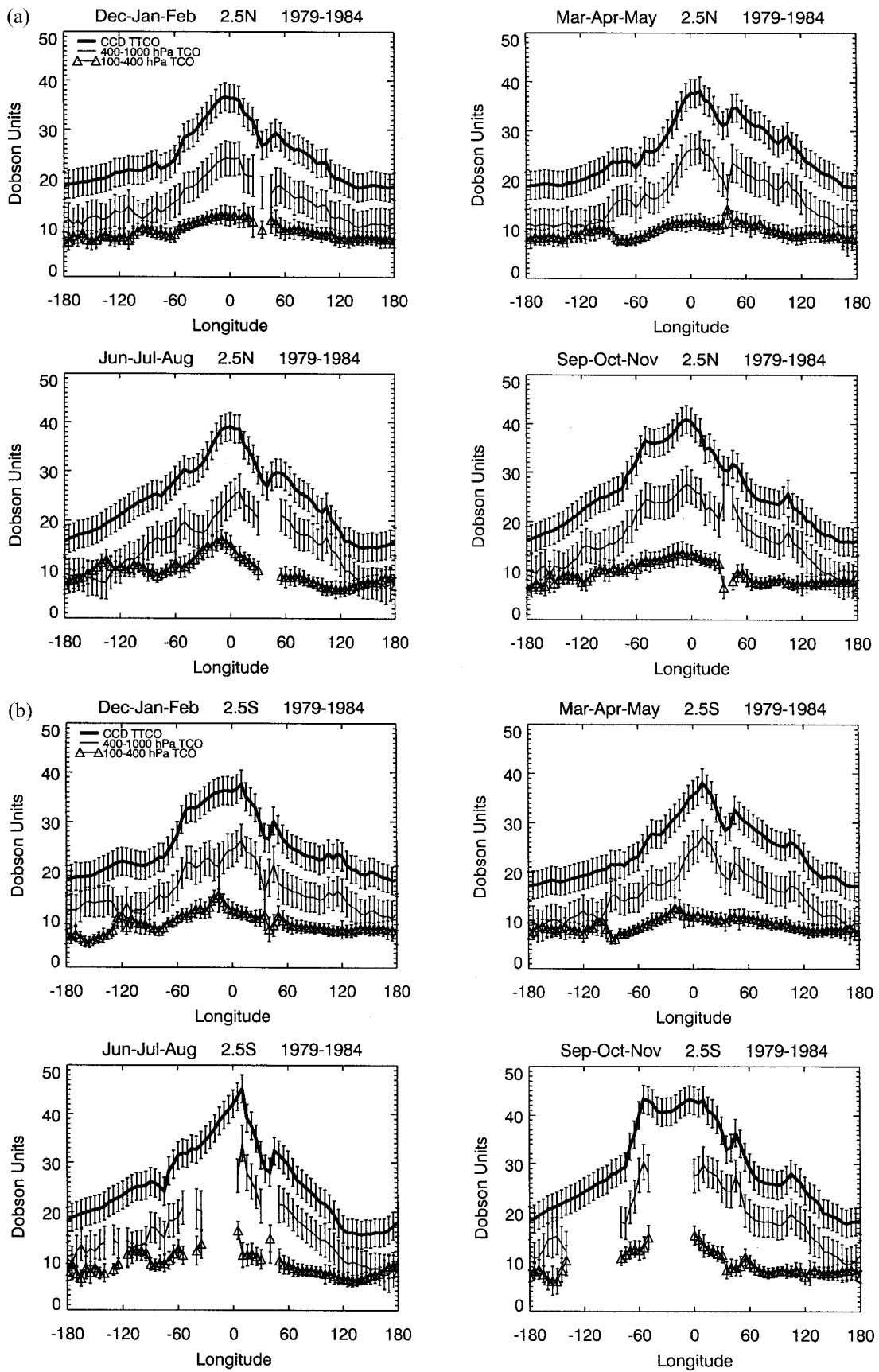


**Figure 5.** Seasonal (3-month seasonal averages indicated in each panel) line plots of convective cloud differential (CCD) derived total tropospheric column ozone (TCO) (top curves), 400- to 1000-hPa column  $O_3$  (middle curves), and 100- to 400-hPa (bottom curves) at (a) latitude  $2.5^\circ N$  and (b) latitude  $2.5^\circ S$ . The data were derived from a 6-year (1979–1984) climatology. The 400- to 1000-hPa column  $O_3$  amounts were derived by subtracting 100- to 400-hPa column  $O_3$  from TCO. Statistical  $\pm 2\sigma$  values are shown for all computed quantities.

100-400 hPa TROPOSPHERIC OZONE (DOBSON UNITS)

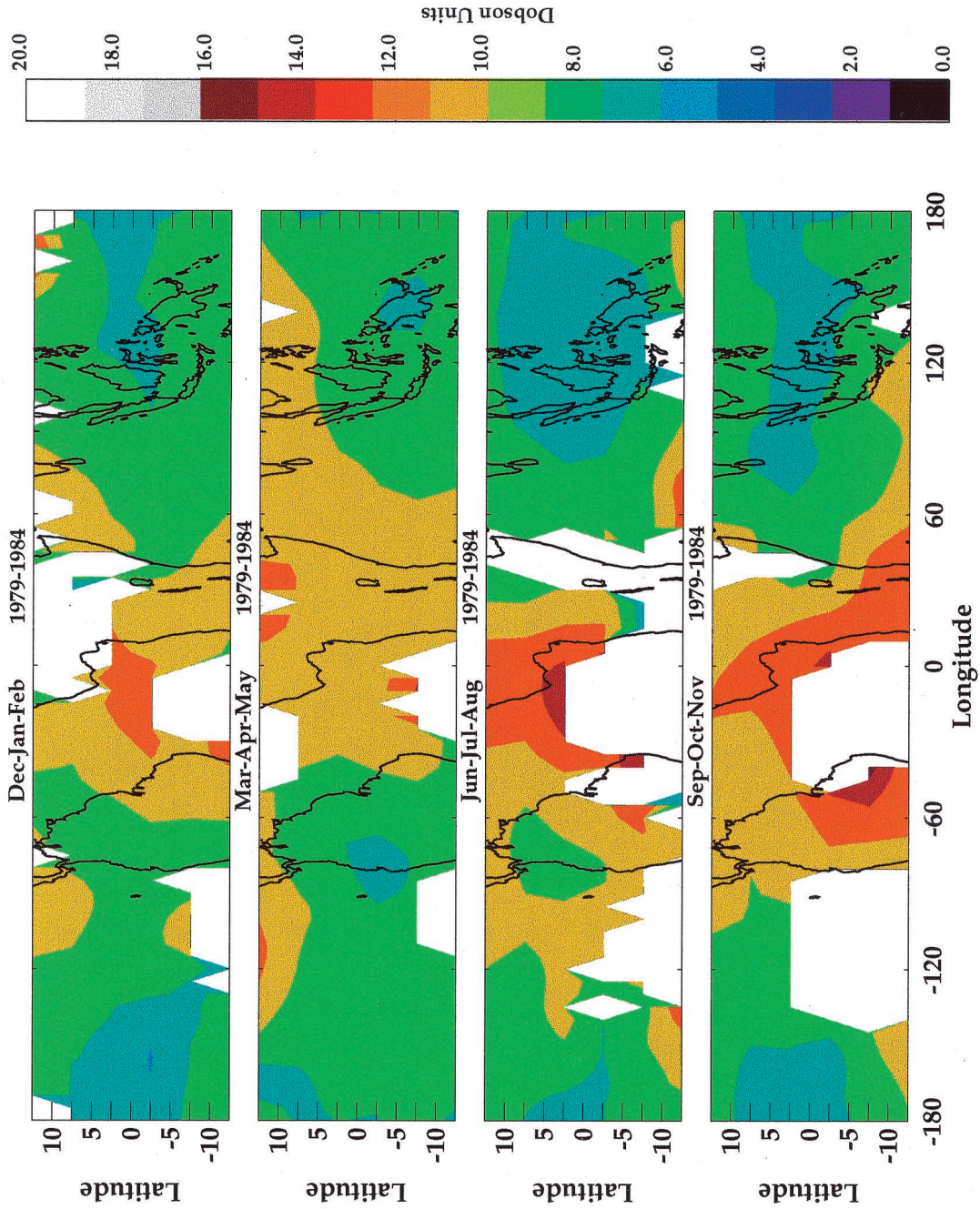


**Plate 1.** Seasonal (3-month seasonal averages indicated in each panel) 6-year (1979–1984) climatology of 100- to 400-hPa column O<sub>3</sub> (in Dobson units) derived from cloud slicing. Column O<sub>3</sub> was calculated by regression line fitting of all TOMS above-cloud column O<sub>3</sub> and THIR cloud-top pressure data pairs lying within the 100- to 400-hPa pressure band.

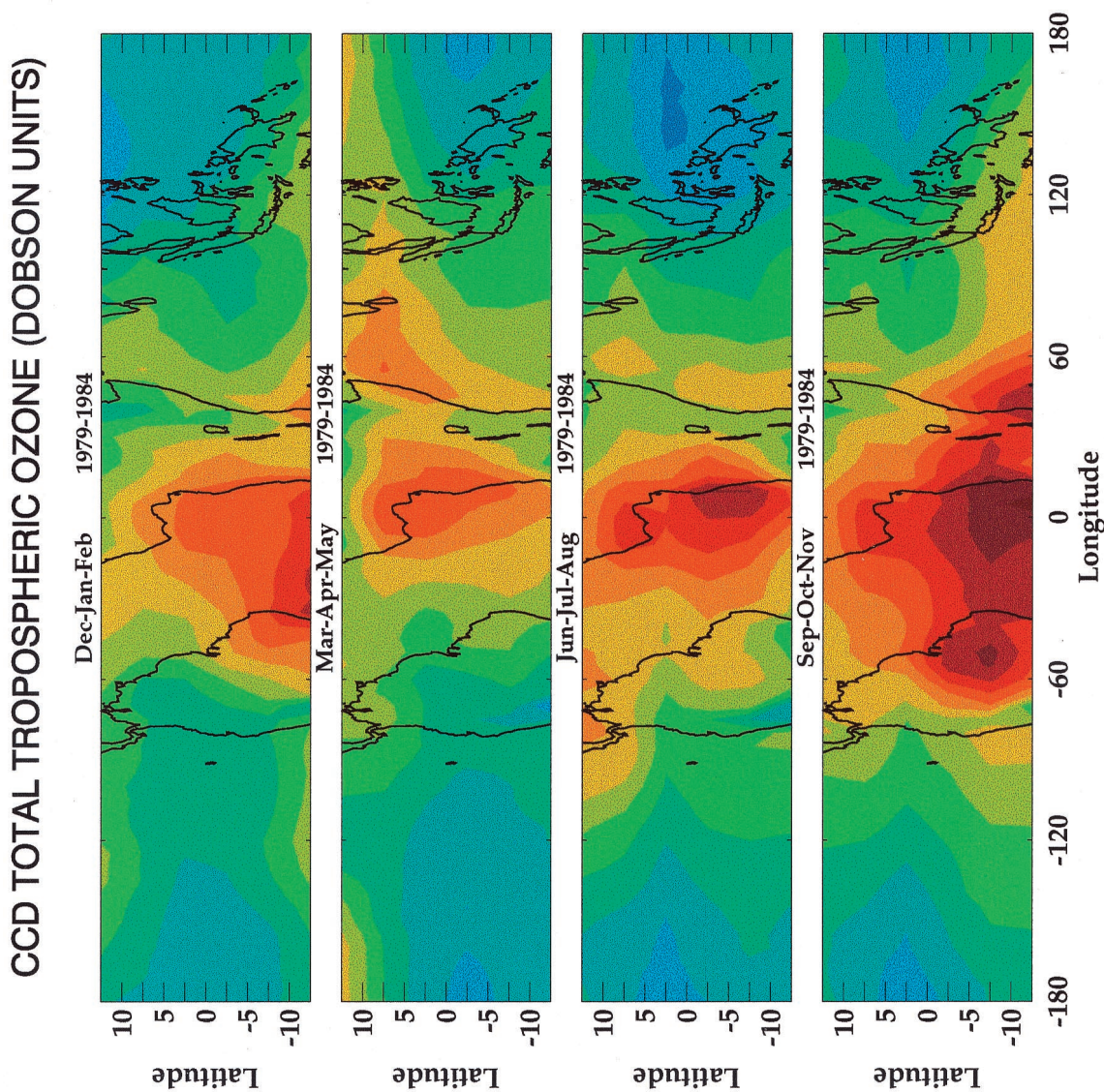


**Plate 2.** Seasonal (3-month seasonal averages indicated in each panel) 6-year (1979–1984) climatology of CCD-derived TCO (in Dobson units).

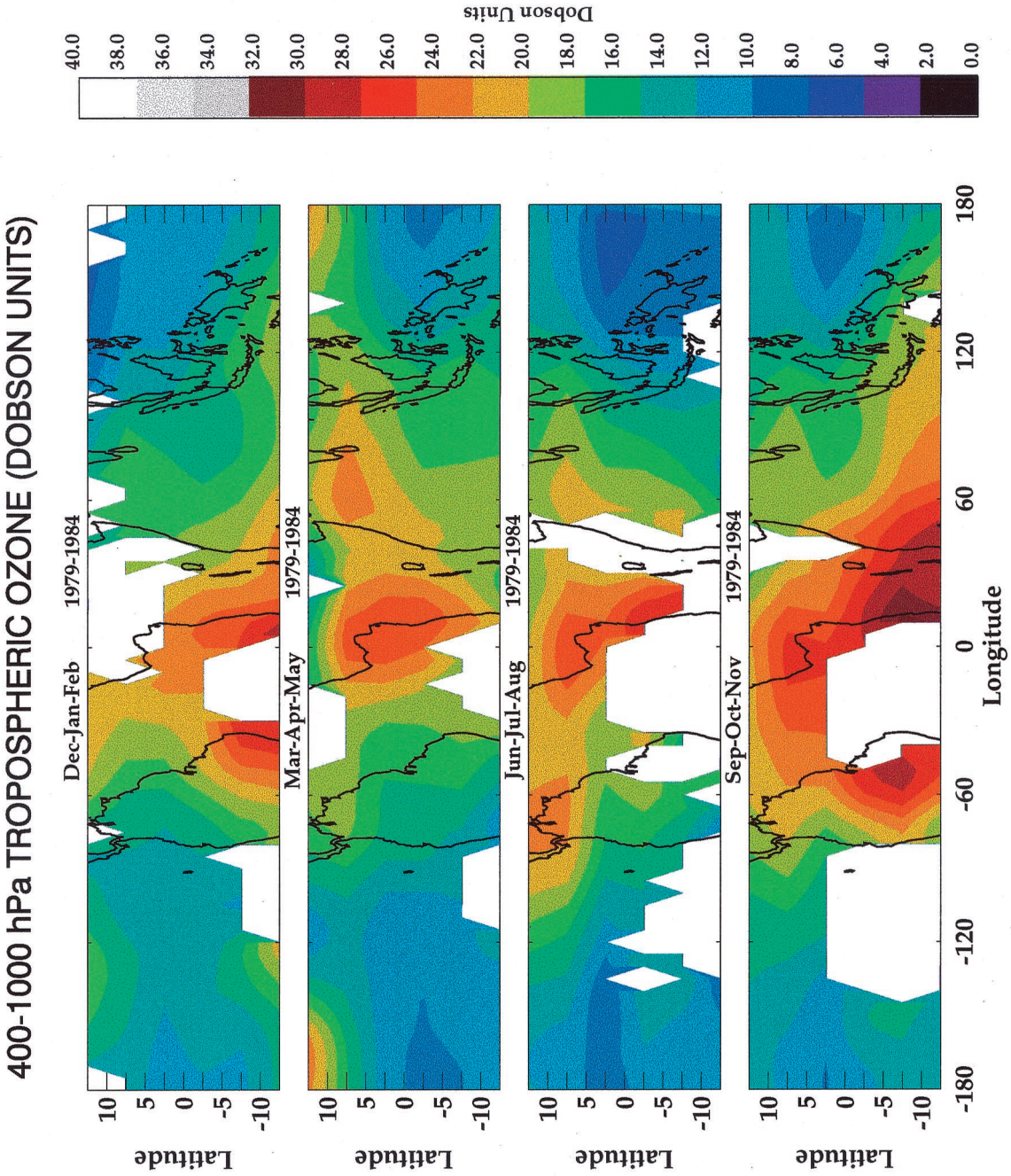


**Plate 3.** Seasonal (3-month seasonal averages indicated in each panel) 6-year (1979–1984) climatology of 400- to 1000-hPa column  $O_3$  (in Dobson units). The data were derived by subtracting 100- to 400-hPa column amounts (shown in Plate 1) from collocated CCD-derived TCO measurements in Plate 2.

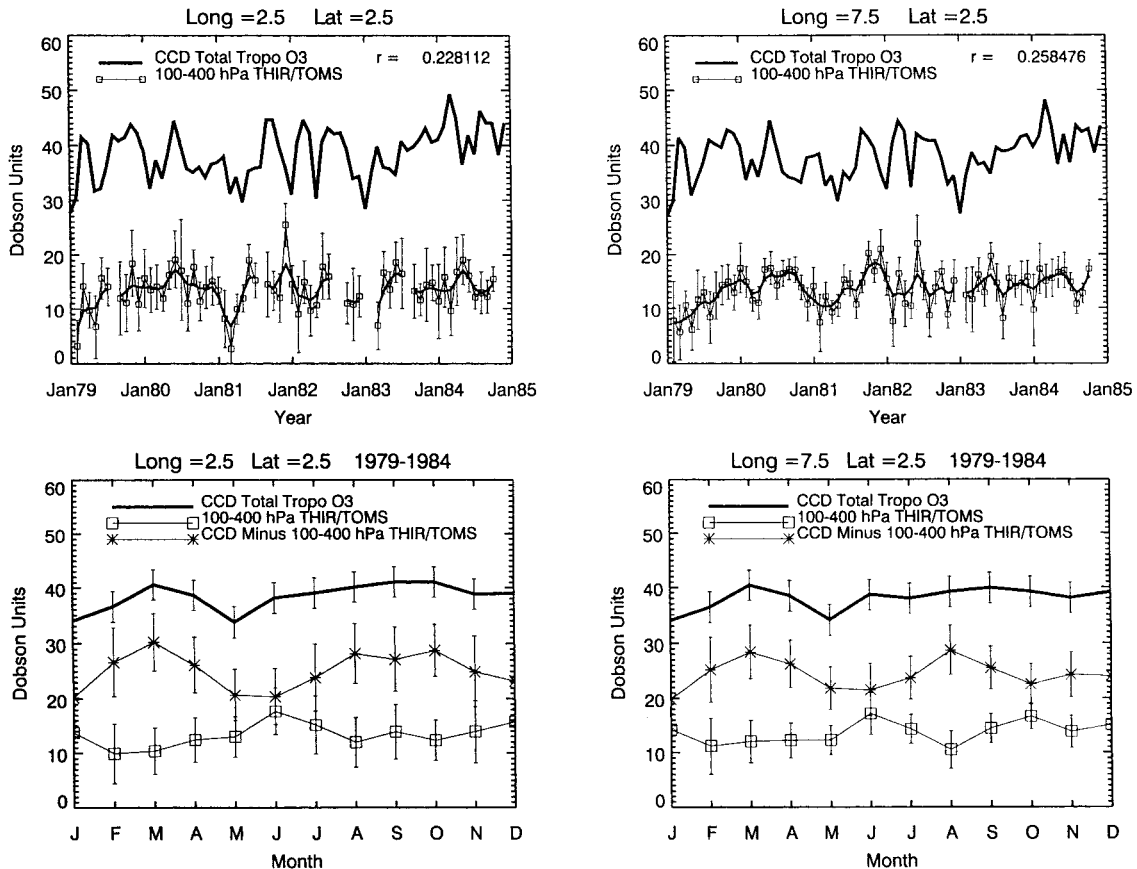


**Figure 6.** (top) Two nearby time series of CCD-derived TCO (top curves) and 100- to 400-hPa column  $O_3$  from cloud slicing (bottom curves) for a region (indicated) off the west coast of equatorial Africa. Time series for the 100- to 400-hPa column  $O_3$  were digitally low-pass filtered (shown in bold) with half-frequency response at 5 months. Statistical  $\pm 2\sigma$  values for the 100- to 400-hPa column  $O_3$  are shown. For TCO,  $2\sigma$  is approximately 5 DU. (bottom) Climatologies corresponding to the above two time series. Shown are TCO (top curves), 400- to 1000-hPa column  $O_3$  (middle curves), and 100- to 400-hPa column  $O_3$  (bottom curves) climatologies. Statistical  $\pm 2\sigma$  values are indicated.

lantic and South Pacific west of Peru which do not have data because there are not enough clouds in the upper troposphere to provide reliable estimates of  $O_3$  from ensemble cloud slicing (see Figure 3). Plate 1 shows a dominant zonal wave number 1 pattern each season with largest  $O_3$  amounts in the Atlantic. The wave number 1 pattern in TCO (e.g., Plate 2) was first identified by *Fishman et al.* [1990] by subtracting SAGE SCO from TOMS total column  $O_3$ . In Plate 1 the persistent wave number 1 pattern in 100- to 400-hPa column  $O_3$  is largest in the June–August and September–November seasons, similar to the seasonal behavior in Plate 2 for TCO.

Regional patterns and seasonal cycles in lower tropospheric column  $O_3$  are shown in Plate 3 and were derived by subtracting column amounts in Plate 1 from column amounts in Plate 2. The horizontal patterns in lower tropospheric column  $O_3$  in Plate 3 show a ubiquitous zonal wave number 1 pattern with the largest column amounts in the September–November season over Brazil in South America and southern Africa. There also appears to be regional increases over the northern region of South America in June–August and off the west coast of equatorial Africa in the March–May season.

## 5. Time Series and Seasonal Cycles

Time series for the region off the west coast of equatorial Africa are illustrated in Figure 6. For better visualization of

seasonal and interannual variabilities the time series for 100- to 400-hPa column  $O_3$  were also digitally low-pass filtered (shown in bold) with half-frequency response at 5 months. The climatologies (bottom panels) indicate within statistical uncertainties that the relative increase in northern spring season TCO may be the result of lower tropospheric  $O_3$ , since upper tropospheric column  $O_3$  from cloud slicing shows no such increase. A relative increase in lower tropospheric column  $O_3$  may also be present in August–October months.

Figure 7 shows time series over western Brazil in South America where there is a more persistent seasonal cycle in TCO. The upper panels in Figure 7 show large increases in TCO around September and secondary maxima around March each year. Upper tropospheric column  $O_3$  (bottom curves) indicate large increases around September each year but no increase in March. As the lower two panels in Figure 7 imply, the March increase in TCO within statistical uncertainties may be attributed to increases in lower tropospheric  $O_3$ . A similar conclusion was noted for Figure 6 for the region west of equatorial Africa.

For the northern region of South America a similar seasonal cycle pattern appears in TCO, as shown in Figure 8. The largest TCO amounts occur during August and September with a secondary maximum in March. The upper and lower tropospheric column  $O_3$  climatology series in Figure 8 imply

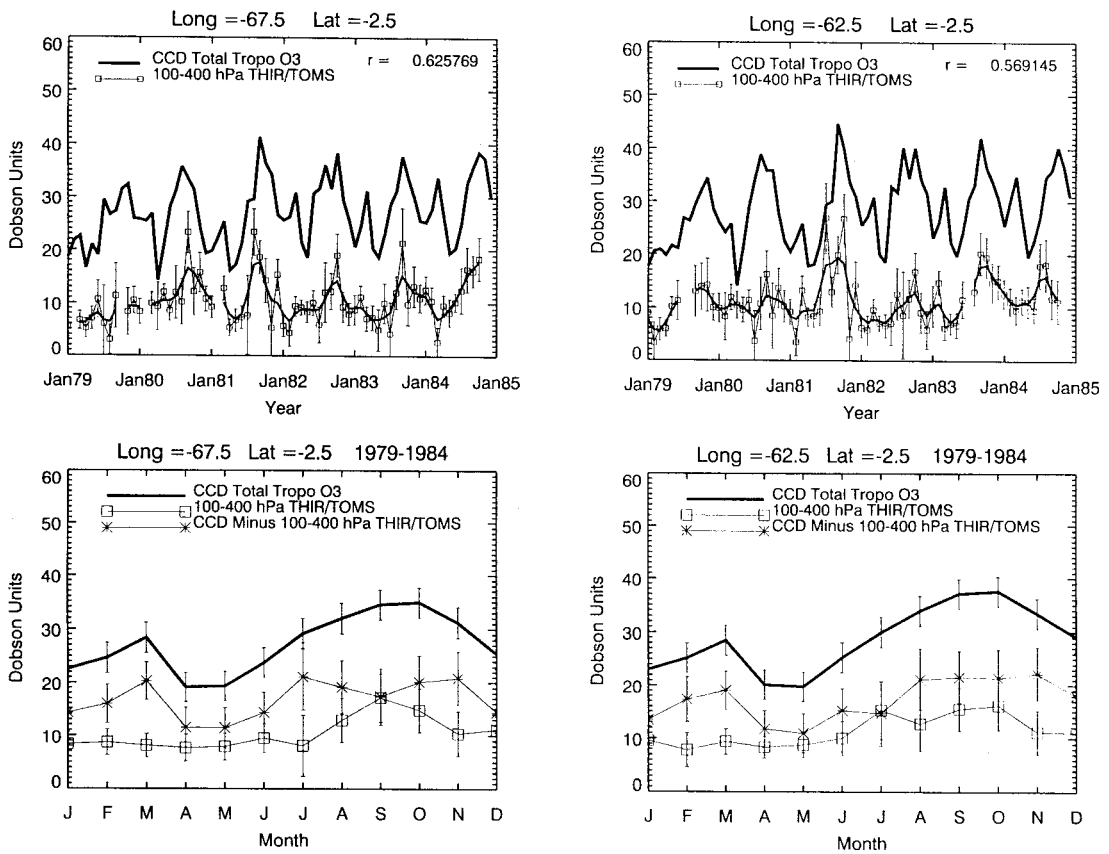


Figure 7. Same as Figure 6 but for a region (indicated) in equatorial western South America.

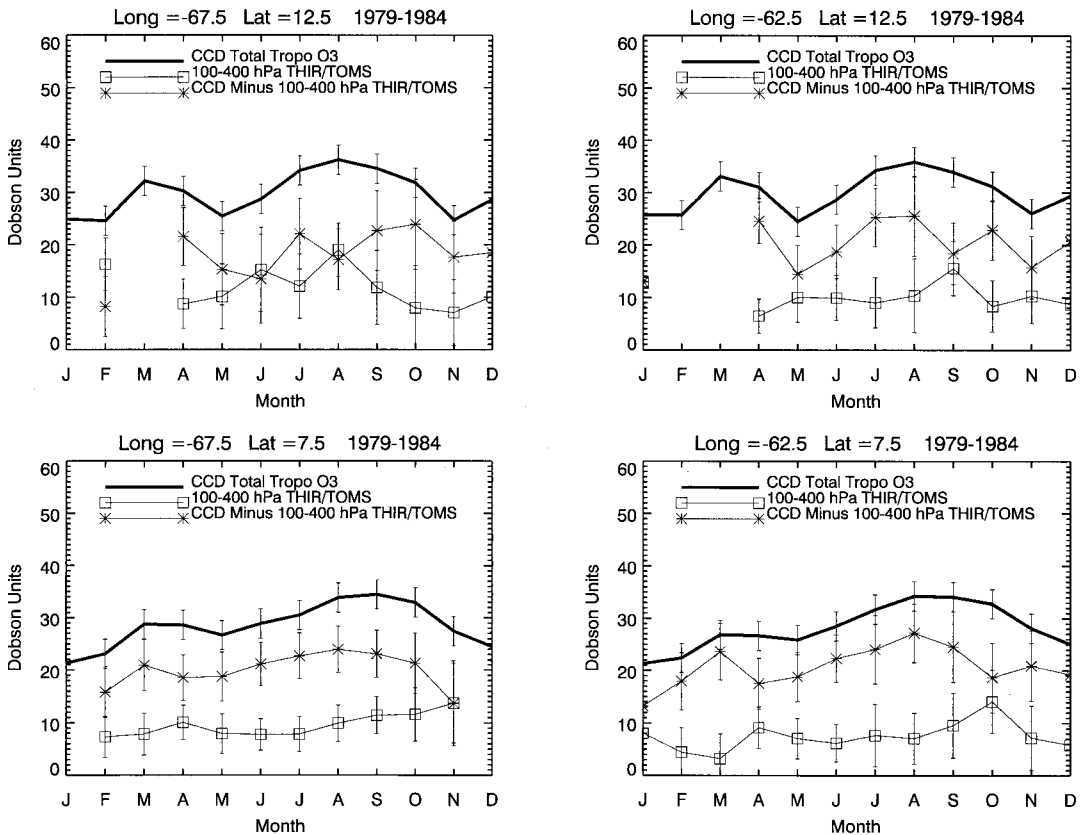


Figure 8. Twelve-month climatologies corresponding to four nearby regions in the northern part of South America. Shown are CCD-derived TCO (top curves), 400- to 1000-hPa column  $O_3$  (middle curves), and 100- to 400-hPa column  $O_3$  (bottom curves) climatologies. Statistical  $\pm 2\sigma$  values are indicated.

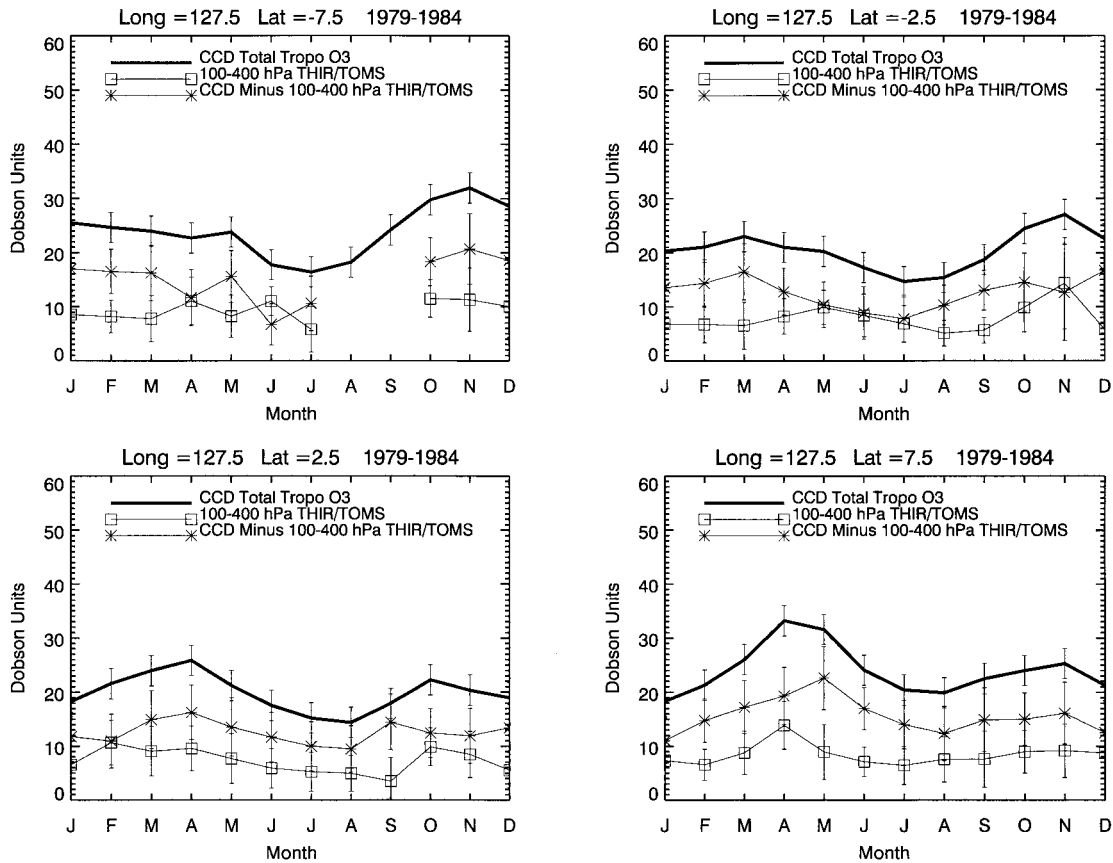


Figure 9. Same as Figure 8 but for four nearby regions in the western Pacific.

that the increase in March likely comes from the lower troposphere.

Seasonal cycles in tropospheric  $O_3$  over the Pacific Ocean provide insight to the impact of differing land-ocean convection systems and topographic influence. Figures 9 and 10 show seasonal cycles in tropospheric column  $O_3$  over the western Pacific (Figure 9) and eastern Pacific (Figure 10). In Figure 9, over the western Pacific where there is influence from land-ocean contrast and seasonal monsoon developments, there are strong seasonal cycles present between hemispheres. The largest TCO abundances appear in the spring months in both hemispheres. Upper and lower tropospheric column  $O_3$  within statistical uncertainties shows similar seasonal cycles.

Figure 10 illustrates seasonal variabilities over a broad zonal region in the eastern Pacific at  $7.5^\circ\text{N}$ . This latitude was chosen as an example because of a significant number of clouds present for developing time series from cloud slicing (see Figure 3). Upper, lower, and total column  $O_3$  measurements all appear to have weak seasonal variability over the eastern Pacific. Weak seasonal variability was indicated by Ziemke *et al.* [1998] in CCD-derived TCO throughout the eastern Pacific and ozonesonde measurements from Samoa ( $14^\circ\text{S}$ ,  $170^\circ\text{W}$ ).

Validation of column  $O_3$  amounts from cloud slicing includes comparison with ozonesonde measurements. For the 1979–1984 time period, only ozonesonde data from Natal ( $5^\circ\text{S}$ ,  $35^\circ\text{W}$ ) exist in the tropics to compare with cloud-slicing column amounts. Figure 11 shows Natal ozonesonde and cloud-slicing column  $O_3$  amounts centered at grid point  $2.5^\circ\text{S}$ ,  $32.5^\circ\text{W}$ . Because of the dry season in Brazil, several months of data from

cloud slicing in Figure 11 are missing because there were too few clouds present for reliable cloud-slicing results.

## 6. Summary

Cloud slicing as presented in this study is the first to distinguish between upper and lower tropospheric  $O_3$  from satellite measurements. All previous methods using satellite data could only estimate the total column of  $O_3$  in the troposphere. Co-located measurements of above-cloud column  $O_3$  from the TOMS instrument were combined with THIR cloud-top pressure data on the Nimbus 7 satellite platform for the period 1979–1984 to derive  $O_3$  abundances in the upper troposphere. Using a residual subtraction method with 100- to 400-hPa upper tropospheric column  $O_3$  from cloud slicing and CCD-derived TCO, it was possible to estimate column  $O_3$  in the lower troposphere (400–1000 hPa) and study its temporal and spatial variabilities.

The analyses indicate a persistent zonal wave number 1 pattern for both lower and upper tropospheric column  $O_3$ , with the largest amounts in the Atlantic region with  $\sim 15$  DU in the 100- to 400-hPa pressure band and  $\sim 25$ – $30$  DU in the 400- to 1000-hPa pressure band. Column  $O_3$  derived from cloud slicing in the 100- to 400-hPa pressure band shows the largest column amounts in the Atlantic region in the June–August and September–November seasons. This seasonal variability is similar to the seasonal variability of TCO in the region. For the lower troposphere the largest column amounts occur around September–November over Brazil and southern Africa. Regional

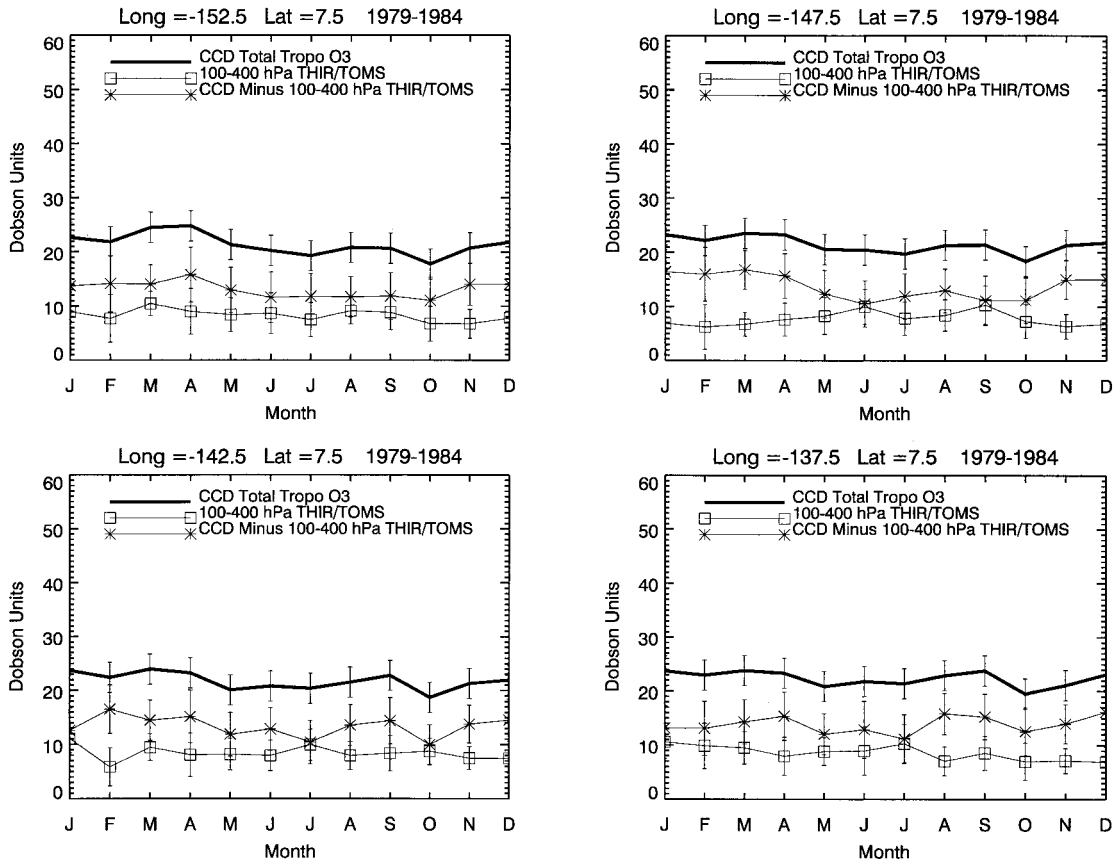


Figure 10. Same as Figure 8 but for four nearby regions in the eastern Pacific.

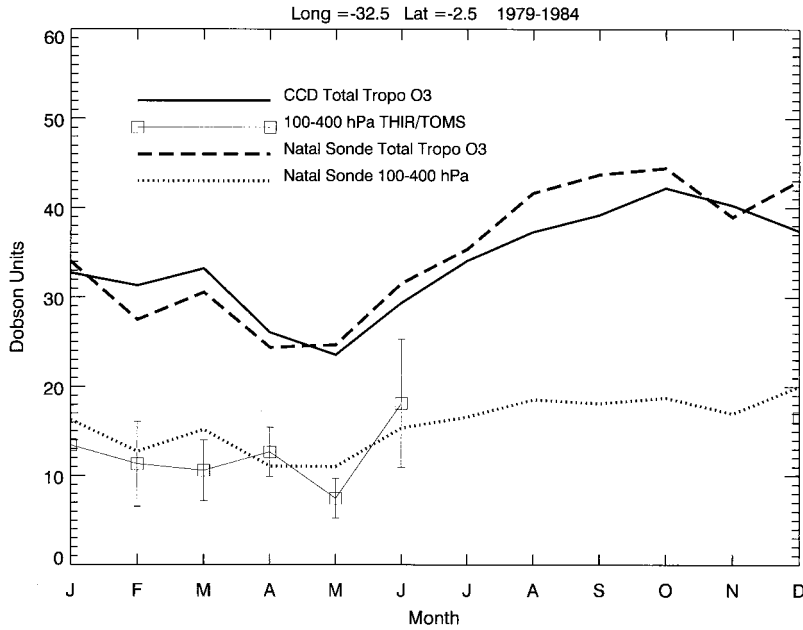


Figure 11. Natal (5°S, 35°W) ozonesonde (dotted and dashed curves) and cloud-slicing column O<sub>3</sub> (squares) 1979–1984 climatology amounts centered at grid point 2.5°S, 32.5°W. Also shown is the coincident CCD-derived TCO climatology (bold curve).

increases in lower tropospheric  $O_3$  appear over the northern region of South America centered around August. Increases were also indicated off the west coast of equatorial Africa in the March–May season.

Several regions in South America and Africa indicate increases in  $O_3$  in the lower troposphere around March. This increase in March was not seen in upper tropospheric column  $O_3$  from cloud slicing. In the eastern Pacific, there is weak seasonal variability of upper, lower, and total tropospheric column  $O_3$  compared with the western Pacific. In the western Pacific the largest TCO amounts occur in the spring months in both hemispheres. In the western Pacific,  $O_3$  variability may be affected by strong convection, pollution and biomass burning, land-sea contrast, and associated seasonal monsoon developments.

For Nimbus 7 TOMS the FOV footprints are large ( $\sim 100$  km diameter, on average), which affects the accuracy and amount of cloud-slicing measurements in this study. Future satellite platforms will have significantly smaller footprint sizes and also improved cloud-top pressure measurements including the rotational Raman scattering ring effect [Joiner and Bhartia, 1995; Joiner et al., 1995], which directly measures colocated cloud-top pressures from single-instrument TOMS measurements. It is anticipated that future work with cloud slicing will include extending this method to outside the tropics and the incorporation of other current and future  $O_3$  and cloud measurement platforms. Future planned  $O_3$  measuring instruments include QuikTOMS (scheduled to be launched in 2001) and the ozone monitoring instrument (OMI) on board the EOS Aura satellite. The OMI will have greater horizontal resolution (about  $13 \times 24$  km at Nadir) than TOMS platforms and several hundred wavelength channels (compared with only six for Nimbus 7 TOMS) for anticipated improvements in the retrieval of  $O_3$ . The EOS Aura platform should provide greatly improved colocated measurements of cloud-top pressure and above-cloud column  $O_3$  (from OMI) for cloud slicing compared with the Nimbus 7 results shown in this pilot study.

## Appendix A: Corrections Made to CCD-Derived TCO

TOMS measurements have several sizable intrinsic errors that should be corrected when deriving TCO. Listed below are three primary corrections made to tropical CCD TCO data used in this investigation. The validation of the CCD data is discussed by Ziemke et al. [1998] and further by Ziemke and Chandra [1999]. These previous studies compared the CCD data with ozonesonde and satellite measurements from the UARS MLS and from HALOE.

### A1. Aerosols

Absorbing aerosols (mostly dust and smoke) in the troposphere absorb backscattered UV radiance and change the  $O_3$  spectral dependence. As a result, the TOMS algorithm underestimates the true total column  $O_3$  content in the presence of absorbing aerosols. An aerosol adjustment was made to all CCD data in this study using the linear technique established by Torres and Bhartia [1999]. With this method, adjustments ( $\Delta\Omega$ ) made to total column  $O_3$  ( $\Omega$ ) are given by  $\Delta\Omega = 0.01K\Omega I$ , where  $I$  is the TOMS aerosol index and  $K$  is a constant equal to 1.12 for Nimbus 7 and 1.2 for Earth Probe. The aerosol adjustment is generally a few Dobson units; however, large adjustments exceeding +10 DU can occur because

of optically thick desert dust or smoke coming from intense wildfires. The largest adjustments (in climatology) in TOMS global monthly averaged data lie over northern Africa (from both desert dust and smoke from biomass burning), with changes of around +8 DU, and along the west coast of central Africa (smoke from biomass burning), with values of around +6 DU.

### A2. Sea Glint

The aerosol adjustment applied to the CCD monthly data also partially corrects for sea glint errors over ocean (Z. Ahmad and O. Torres, personal communication, 2000). The sea glint effect is a function of solar declination and is caused by bright surface reflection. For a scene affected by clear-sky sea glint, TOMS underdetermines the true total column  $O_3$  content. Sea glint can cause errors of about  $-5$  to  $-10$  DU in daily measurements and about  $-1$  to  $-3$  DU in monthly means.

### A3. Retrieval Efficiency

Because of strong Rayleigh scattering at UV wavelengths, the TOMS instrument has reduced sensitivity to  $O_3$  in the lower troposphere below about 5 km altitude [e.g., Klenk et al., 1982; Hudson et al., 1995]. Although the TOMS algorithm includes a lower tropospheric efficiency correction, it is based on a climatology. Hence values of column  $O_3$  greater than or smaller than a certain number (about 35 DU in TCO) require adjustment. For the CCD-derived TCO monthly data, a first-order efficiency correction was applied. In an effort to provide an efficiency correction, there must first be a clear functional relationship identified between lower tropospheric  $O_3$  and TCO. This relationship to first-order is a straight line. Figure A1 is a plot of 0- to 5-km column  $O_3$  ( $\Omega_{0-5 \text{ km}}$ ) versus TCO ( $\Omega_{\text{TCO}}$ ) derived from  $O_3$  profiles from a number of tropical sonde stations. These sonde measurements have been operating under the Southern Hemisphere Additional Ozonesondes (SHADOZ) ([http://code916.gsfc.nasa.gov/Data\\_services/Data.html](http://code916.gsfc.nasa.gov/Data_services/Data.html)). Shown is a linear fit  $\Omega_{0-5 \text{ km}} = \beta\Omega_{\text{TCO}}$  to the data which indicates a slope  $\beta = 0.43 \pm 0.013(2\sigma)$ . Hence, on average, when TCO changes by +1 DU, 0- to 5-km column  $O_3$  changes by about +0.43 DU.

The TOMS algorithm assumes about 15 DU for 0- to 5-km column  $O_3$  in the tropics. A first-order efficiency correction ( $\Delta\Omega_{\text{TCO}}$ ) for initially measured CCD TCO ( $\Omega_{\text{TCO}}$ ) is given by  $\Delta\Omega_{\text{TCO}} = \varepsilon[\beta\Omega_{\text{TCO}} - 15]$ , where  $\beta$  is the slope in Figure A1 and  $\varepsilon$  is a retrieval efficiency parameter for TOMS 0- to 5-km column  $O_3$ . However,  $\Omega_{\text{TCO}}$  is presumably not correct as measured by the CCD method, so to first-order we derive a new value for  $\Omega_{\text{TCO}}$  by  $\Omega_{\text{TCO}} \rightarrow \Omega_{\text{TCO}} + \Delta\Omega_{\text{TCO}}$ , which yields a new value for  $\Omega_{\text{TCO}}$  given by  $[1 + \beta\varepsilon]\Omega_{\text{TCO}} - 15\varepsilon$ . Substituting this into the expression for  $\Delta\Omega_{\text{TCO}}$  yields a final first-order correction for TCO given by  $\Delta\Omega_{\text{TCO}} = \beta\varepsilon[1 + \beta\varepsilon]\Omega_{\text{TCO}} - 15\beta\varepsilon^2 - 15\varepsilon$ . For altitude range 0–5 km,  $\beta = 0.43$  and  $\varepsilon = 0.5$ , and this yields  $\Delta\Omega_{\text{TCO}} = 0.26\Omega_{\text{TCO}} - 9.1$  DU. Note that the correction to  $\Omega_{\text{TCO}}$  is zero for  $\Omega_{\text{TCO}} = 35$  DU (i.e.,  $9.1/0.26 = 35$  DU). Adjustments for monthly CCD data were found to be, on average (in climatology), at most about 2–3 DU (around +2 to +3 DU adjustment in the Atlantic and  $-2$  to  $-3$  DU adjustment over the Pacific).

## Appendix B: Partial Column Ozone Calculation for the Upper Troposphere

Because the number 0.79 in (1) is not a true constant but varies with altitude, we provide a detailed derivation of this

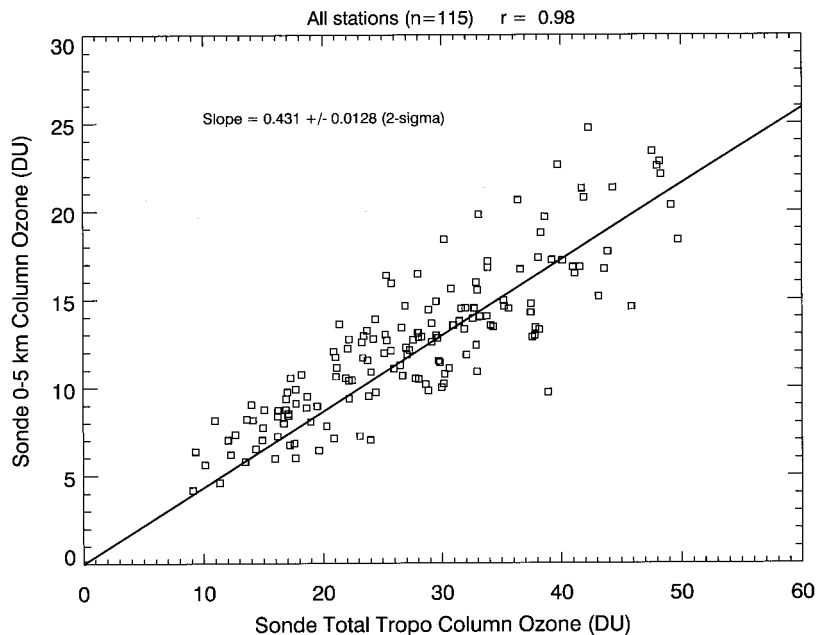


**Figure A1.** Partial column  $O_3$  for the altitude range 0–5 km plotted versus total tropospheric column  $O_3$ . These column  $O_3$  amounts were derived from Southern Hemisphere Additional Ozonesondes (SHADOZ)  $O_3$  ozonesonde profile measurements. The number of profiles is 115, involving eight tropical stations for 1995–1999. Also shown is a linear fit to the data which indicates a slope  $0.43 \pm 0.013(2\sigma)$ . Correlation  $r$  is  $+0.98$ .

equation as applied specifically to the evaluation of column  $O_3$  measurements in the upper troposphere. Total column  $O_3$  ( $\Omega$ ) expressed in Dobson units is the equivalent vertical thickness of all atmospheric  $O_3$  over an arbitrary horizontal surface area ( $S$ ) over the Earth under conditions of standard temperature ( $T_{STD} = 273.16$  K) and standard pressure ( $P_{STD} = 101325$  Pa) [e.g., Andrews *et al.*, 1987]. One Dobson unit is equivalent to  $10^{-5}$  m vertical thickness of this volume element and a horizontal surface density of  $2.69 \times 10^{20}$   $O_3$  molecules  $m^{-2}$ .

The scheme for deriving (1) lies in the determination of horizontal surface density. The horizontal surface density follows by applying the ideal gas law ( $P = nk_B T$ , where  $P$  is pressure, in pascals,  $n$  is total number of molecules per cubic meter in the atmosphere,  $k_B$  is Boltzmann's constant, equal to  $1.3806 \times 10^{-23}$  J  $K^{-1}$ , and  $T$  is absolute temperature, in kelvins) to this volume element ( $N_{O_3}$  is the total number of  $O_3$  molecules in this volume element of volume  $S\Omega$ ):

$$\frac{N_{O_3}}{S} = \frac{P_{STD}}{k_B T_{STD}} \Omega. \quad (B1)$$

When  $\Omega$  is set equal to 1 DU (i.e.,  $10^{-5}$  m), the right-hand side of (B1) yields a horizontal surface density of  $2.69 \times 10^{20}$   $O_3$  molecules  $m^{-2}$ .

The integral formula (1) then follows by deriving an integral expression for the horizontal surface density and setting this equal to the right-hand side of (B1). Given  $O_3$  volume mixing ratio  $X$ , the total number of  $O_3$  molecules contained in the volume element is given by ( $V$  is volume and  $z$  is altitude)

$$N_{O_3} = \int_V dV n_{O_3} \quad (B2)$$

$$N_{O_3} = \int_V dV nX \quad (B3)$$

$$N_{O_3} = S \int_0^{\infty} dz nX, \quad (B4)$$

where it is understood that the contribution to the integral in (B4) comes from a thin layer in  $z$  about the mean altitude of the surface  $S$ .

Using the hydrostatic relation ( $dP/dz = -\rho g$ , where  $P$  is pressure,  $\rho$  is mass density, and  $g$  is acceleration of gravity), it follows that

$$N_{O_3} = S \int_0^{P_s} \frac{dP \rho N_A}{g \rho \mu} X, \quad (B5)$$

where  $N_A$  is Avagadro's number ( $6.022 \times 10^{26}$  molecules  $kmol^{-1}$ ) and  $\mu$  is the mean molecular weight of the atmosphere (approximately 29 for both the troposphere and stratosphere). The horizontal surface density of  $O_3$  molecules is then given by

$$\frac{N_{O_3}}{S} = \frac{N_A}{\mu} \int_0^{P_s} \frac{dP}{g} X. \quad (B6)$$

Setting the right-hand sides of (B1) and (B6) equal, it follows that total column  $O_3$  is given by

$$\Omega = \frac{k_B T_{STD} N_A}{\mu P_{STD}} \int_0^{P_s} \frac{dP}{g} X. \quad (B7)$$

From (B7), partial column  $O_3$  in the upper troposphere is then calculated from

$$\Omega = \frac{k_B T_{STD} N_A}{\mu P_{STD} \langle g \rangle} \int_{P_{low}}^{P_{high}} dP X, \quad (B8)$$

where  $\langle g \rangle$  is the mean acceleration of gravity ( $\langle g \rangle \approx 9.76 \text{ m s}^{-2}$ ) for the upper troposphere between pressure levels  $P_{low}$  and  $P_{high}$ . Substitution of all parameter values in (B8) yields the number  $0.79 \text{ DU hPa}^{-1} \text{ ppmv}^{-1}$  out front of the integral when  $P$  is in hectopascals (equivalent to millibars) and  $X$  is in parts per million by volume (ppmv). The number 0.79 in (B8) applies to the upper troposphere, but even for the stratosphere this number is only marginally larger, up to  $\sim 0.80$  around the stratopause ( $\sim 50 \text{ km}$  altitude) because of a slightly reduced mean value for  $\langle g \rangle$ . Calculation of absolute (troposphere plus the atmosphere above) total column  $O_3$  with the number 0.79 in (B8) will produce only small errors (i.e., underestimates) of at most about 1%.

**Acknowledgments.** We thank Anne Thompson for expertise with managing the SHADOZ project and the many individuals involved in it, including Sam Oltmans and Frank Schmidlin, and also Jacquelyn Witte for providing all of the SHADOZ data in an easy user format.

## References

- Andrews, D. G., J. R. Holton, and C. B. Leovy, *Middle Atmosphere Dynamics*, 489 pp., Academic, San Diego, Calif., 1987.
- Basist, A. N., and M. Chelliah, Comparison of tropospheric temperatures derived from the NCEP/NCAR reanalysis, NCEP operational analysis, and the microwave sounding unit, *Bull. Am. Meteorol. Soc.*, **78**, 1431–1447, 1997.
- Basist, A. N., C. F. Ropelewski, and N. C. Grody, Comparison of tropospheric temperature derived from the microwave sounding unit and the National Meteorological Center analysis, *J. Clim.*, **8**, 668–681, 1995.
- Chandra, S., J. R. Ziemke, W. Min, and W. G. Read, Effects of the 1997–1998 El Niño on tropospheric ozone and water vapor, *Geophys. Res. Lett.*, **25**, 3867–3870, 1998.
- Eck, T. F., P. K. Bhartia, P. H. Hwang, and L. L. Stowe, Reflectivity of Earth's surface and clouds in ultraviolet from satellite observations, *J. Geophys. Res.*, **92**, 4287–4296, 1987.
- Fishman, J., and A. E. Balok, Calculation of daily tropospheric ozone residuals using TOMS and empirically improved SBUV measurements: Application to an ozone pollution episode over the eastern United States, *J. Geophys. Res.*, **104**, 30,319–30,340, 1999.
- Fishman, J., C. E. Watson, J. C. Larsen, and J. A. Logan, Distribution of tropospheric ozone determined from satellite data, *J. Geophys. Res.*, **95**, 3599–3617, 1990.
- Fishman, J., V. G. Brackett, E. V. Browell, and W. B. Grant, Tropospheric ozone derived from TOMS/SBUV measurements during TRACE A, *J. Geophys. Res.*, **101**, 24,069–24,082, 1996.
- Hudson, R. D., and A. M. Thompson, Tropical tropospheric ozone (TTO) from TOMS by a modified-residual method, *J. Geophys. Res.*, **103**, 22,129–22,145, 1998.
- Hudson, R. D., J.-H. Kim, and A. M. Thompson, On the derivation of tropospheric column ozone from radiances measured by the total ozone mapping spectrometer, *J. Geophys. Res.*, **100**, 11,137–11,145, 1995.
- Joiner, J., and P. K. Bhartia, The determination of cloud pressures from rotational Raman scattering in satellite backscatter ultraviolet measurements, *J. Geophys. Res.*, **100**, 23,019–23,026, 1995.
- Joiner, J., P. K. Bhartia, R. P. Cebula, E. Hilsenrath, R. D. McPeters, and H. Park, Rotational Raman scattering (ring effect) in satellite backscatter ultraviolet measurements, *Appl. Opt.*, **34**, 4513–4525, 1995.
- Klenk, K. F., P. K. Bhartia, A. J. Fleig, V. G. Kaveeshwar, R. D. McPeters, and P. M. Smith, Total ozone determination from the backscattered ultraviolet (BUV) experiment, *J. Appl. Meteorol.*, **21**, 1672–1684, 1982.
- McPeters, R. D., et al., Nimbus-7 total ozone mapping spectrometer (TOMS) data products user's guide, *NASA Ref. Publ.*, *RP-1384*, 67 pp., 1996.
- Stowe, L.-L., et al., Nimbus-7 global cloud climatology, part I, Algorithms and validation, *J. Clim.*, **1**, 445–470, 1988.
- Stowe, L. L., et al., Nimbus-7 global cloud climatology, part II, First year results, *J. Clim.*, **2**, 671–709, 1989.
- Thompson, A. M., and R. D. Hudson, Tropical tropospheric ozone (TTO) maps from Nimbus 7 and Earth Probe TOMS by the modified-residual method: Evaluation with sondes, ENSO signals, and trends from Atlantic regional time series, *J. Geophys. Res.*, **104**, 26,961–26,975, 1999.
- Torres, O., and P. K. Bhartia, Impact of tropospheric aerosol absorption on ozone retrieval from backscattered ultraviolet measurements, *J. Geophys. Res.*, **104**, 21,569–21,577, 1999.
- Vukovich, F. M., V. Brackett, J. Fishman, and J. E. Sickles II, On the feasibility of using the tropospheric ozone residual for nonclimatological studies on a quasi-global scale, *J. Geophys. Res.*, **101**, 9093–9105, 1996.
- Ziemke, J. R., and S. Chandra, On tropospheric ozone and the tropical wave 1 in total column ozone, *Proc. 18th Quadrenn. Ozone Symp.*, **1**, 447–450, 1998.
- Ziemke, J. R., and S. Chandra, Seasonal and interannual variabilities in tropical tropospheric ozone, *J. Geophys. Res.*, **104**, 21,425–21,442, 1999.
- Ziemke, J. R., and J. L. Stanford, The quasi-biennial oscillation and tropical waves in total ozone, *J. Geophys. Res.*, **99**, 23,041–23,056, 1994.
- Ziemke, J. R., S. Chandra, and P. K. Bhartia, Two new methods for deriving tropospheric column ozone from TOMS measurements: The assimilated UARS MLS/HALOE and convective-cloud differential techniques, *J. Geophys. Res.*, **103**, 22,115–22,127, 1998.

P. K. Bhartia and S. Chandra, NASA Goddard Space Flight Center, Greenbelt, MD 20771.

J. R. Ziemke, Chemistry and Dynamics Branch, NASA Goddard Space Flight Center, Code 916, Building 33, Room E417, Greenbelt, MD 20771. (ziemke@jwocgy.gsfc.nasa.gov)

(Received September 7, 2000; revised November 22, 2000; accepted November 29, 2000.)

